HHS Public Access

Author manuscript

Sci Transl Med. Author manuscript; available in PMC 2016 June 17.

Published in final edited form as:

Sci Transl Med. 2015 June 17; 7(292): 292ra99. doi:10.1126/scitranslmed.aaa5843.

Vinculin network–mediated cytoskeletal remodeling regulates contractile function in the aging heart

Gaurav Kaushik[1,*], **Alice Spenlehauer**[1,†], **Ayla O. Sessions**[2], **Adriana S. Trujillo**[3], **Alexander Fuhrmann**[1], **Zongming Fu**[4], **Vidya Venkatraman**[5], **Danielle Pohl**[1,‡], **Jeremy Tuler**[1], **Mingyi Wang**[6], **Edward G. Lakatta**[6], **Karen Ocorr**[7], **Rolf Bodmer**[7], **Sanford I. Bernstein**[3], **Jennifer E. Van Eyk**[4,5], **Anthony Cammarato**[4,§], and **Adam J. Engler**[1,2,8,§]

[§]Corresponding author. acammar3@jhmi.edu (A.C.); aengler@ucsd.edu (A.J.E.).
[*]Present address: Harvard-MIT Division of Health Sciences and Technology, Massachusetts Institute of Technology; Center for Biomedical Engineering, Department of Medicine, Brigham & Women's Hospital, Harvard Medical School, Cambridge, MA 02139, USA.
[†]Present address: Department of Biomedical Engineering, Imperial College London, London SW7 2AZ, UK.
[‡]Present address: Department of Biology, Iowa State University, Ames, IA 50011, USA.

SUPPLEMENTARY MATERIALS

www.sciencetranslationalmedicine.org/cgi/content/full/7/292/292ra99/DC1

Author contributions: G.K., J.E.V.E., A.C., and A.J.E. designed the experiments and conceived the project; G.K. performed mechanical analyses on flies, immunohistochemistry, and image analysis; G.K., A.S., and A.O.S. performed *Drosophila* husbandry, gene expression analysis, and immunofluorescence microscopy; J.T. performed rat husbandry; G.K., J.T., and D.P. prepared rat samples; G.K. and D.P. designed and created *MhcKD* + *VincHE*; G.K. and A.S.T. designed and performed transmission electron microscopy experiments and analysis; Z.F. performed MS experiments; M.W. performed simian husbandry and isolated simian tissue; G.K., A.F., V.V., A.C., and A.J.E. analyzed experimental data; G.K., V.V., K.O., and R.B. provided data analysis methods; G.K., V.V., and A.C. performed statistical analyses; G.K., E.G.L., K.O., R.B., S.I.B., J.E.V.E., A.C., and A.J.E. wrote and edited the paper.

Competing interests: The authors declare that they have no competing interests.

Data and materials availability: Proteomic data are available via the PRoteomics IDEntifications (PRIDE) database at accession numbers PXD001839 (rat) and PXD001842 (simian).

[1]Department of Bioengineering, University of California, San Diego, La Jolla, CA 92093, USA

[2]Biomedical Sciences Program, University of California, San Diego, La Jolla, CA 92093, USA

[3]Department of Biology, Heart Institute, and Molecular Biology Institute, San Diego State University, San Diego, CA 92182, USA

[4]Division of Cardiology, Department of Medicine, Johns Hopkins University, Baltimore, MD 21205, USA

[5]Advanced Clinical Biosystems Research Institute, Barbra Streisand Women's Heart Center, Cedars-Sinai Heart Institute, Cedars-Sinai Medical Center, Los Angeles, CA 90048, USA

[6]Laboratory of Cardiovascular Science, Intramural Research Program, National Institute on Aging, National Institutes of Health, Baltimore, MD 21224, USA

[7]Development and Aging Program, Sanford-Burnham Medical Research Institute, La Jolla, CA 92037, USA

[8]Sanford Consortium for Regenerative Medicine, La Jolla, CA 92037, USA

Abstract

The human heart is capable of functioning for decades despite minimal cell turnover or regeneration, suggesting that molecular alterations help sustain heart function with age. However, identification of compensatory remodeling events in the aging heart remains elusive. We present the cardiac proteomes of young and old rhesus monkeys and rats, from which we show that certain age-associated remodeling events within the cardiomyocyte cytoskeleton are highly conserved and beneficial rather than deleterious. Targeted transcriptomic analysis in *Drosophila* confirmed conservation and implicated vinculin as a unique molecular regulator of cardiac function during aging. Cardiac-restricted vinculin overexpression reinforced the cortical cytoskeleton and enhanced myofilament organization, leading to improved contractility and hemodynamic stress tolerance in healthy and myosin-deficient fly hearts. Moreover, cardiac-specific vinculin overexpression increased median life span by more than 150% in flies. A broad array of potential therapeutic targets and regulators of age-associated modifications, specifically for vinculin, are presented. These findings suggest that the heart has molecular mechanisms to sustain performance and promote longevity, which may be assisted by therapeutic intervention to ameliorate the decline of function in aging patient hearts.

INTRODUCTION

The average age worldwide is projected to increase markedly in the coming decades. Advanced age is a primary risk factor for cardiac dysfunction and subsequent morbidity and mortality (1). Treating age-related heart failure (HF) is complicated due to its heterogeneous etiologies. A multitude of remodeling events associated with cardiac aging are thought to impair myocardial performance (1, 2). Remodeling fundamentally begins with molecular changes, such as altered cell growth regulation (3) and protein expression (4). Because cardiomyocyte renewal in the heart is limited (5), functional maintenance may depend on molecular remodeling over time- or age-related compensatory responses to minimize

damage. Identifying compensatory aging events is difficult because of diverse aging processes within and between organisms and an abundance of maladaptive events. However, integrated approaches that identify conserved hallmarks of cardiac aging and verify their positive or negative functional consequences can assist in distinguishing therapeutic targets for treating age-related HF or improving outcomes during aging.

The cortical cytoskeleton in cardiomyocytes couples sarcomeres to the membrane at cell-matrix (costameric) and cell-cell junctions [intercalated disc (ID)], translates sarcomeric contraction into cell shortening, and undergoes remodeling in aging patients (6, 7) and during HF (8, 9). Aging may therefore affect mechanotransduction, the signaling induced by changing physical forces, through cytoskeletal proteins. Vinculin, for example, is force-sensitive (10), regulates cell shape (11) and intracellular signaling (12, 13), and is overexpressed in aging patient myocardium (7). Mechanical loading of cardiomyocytes results in reinforcement of cell junctions (11, 14, 15) and increased vinculin-mediated cross-linking of transmembrane proteins to the cortical actin superstructure (15, 16). Conversely, mechanical unloading via left ventricular (LV) assist devices can restore baseline vinculin and cytoskeletal gene expression in HF patients (8, 9), and, moreover, vinculin mutation alone can result in HF (17). These data suggest relationships between the cytoskeleton, ventricular contractility, and ventricular load. Therefore, we hypothesized that vinculin may additionally influence cardiac performance with age. However, conservation of vinculin overexpression in aging model systems and its structural and functional consequences have never been investigated. Therefore, we examined these with complementary techniques in multiple aging systems of varying complexity.

We assessed conservation of known human aging hallmarks and identified novel molecular alterations by analyzing the LV proteomes of adult and aged simians (*Macacca mulatta*) and rats (*Rattus norvegicus*) using mass spectrometry (MS). Subsequent investigations suggested that the vinculin network has a central, conserved role in cardiac aging. Using *Drosophila melanogaster*, a rapidly aging and genetically tractable model system, we observed that cardiac vinculin overexpression induced extensive cytoskeletal and cellular remodeling and correlated with enhanced cardiac contractility and life span extension. In contrast to a perception that remodeling is predominantly maladaptive, these data strongly suggest a beneficial role for vinculin overexpression in the aging heart. We demonstrate vinculin-mediated cytoskeletal remodeling as a compensatory mechanism in which tensional homeostasis is altered to preserve cardiac function during aging. Vinculin network proteins may thus serve as potent therapeutic targets for improving HF patient outcome.

RESULTS

Simian and murine ventricles exhibit age-related cytoskeletal remodeling

Proteomic quantification of LV free wall myocardial samples from adult and aged rhesus monkeys (11 and 22 years, respectively) and rats (6 and 24 months, respectively) was performed using MS (Fig. 1A). Tryptic peptides (tables S1 and S2) and a total of 1206 (simian) and 1086 (rat) nonredundant proteins (tables S3 and S4) were quantified; of these proteins, 602 were common between species. On the basis of STRAP (Software Tool for Rapid Annotation of Proteins) analysis (18) of the cellular compartments in both proteomes,

cytoskeletal proteins were among the most plentiful groups in monkeys and rats, regardless of gender and age ratios (fig. S1 and table S5). The most abundant biological functions in both species involved molecules with a role in subcellular organization, or formation and maintenance of intracellular and/or organelle structure (fig. S1 and table S6). On the basis of label-free quantification via normalized spectral counts, proteins involved in the cytoskeleton and cell organization increased in quantity with age, especially in monkeys (Fig. 1B). These proteins were associated with cardiac biological functions, including cardiovascular disease (table S7), and numerous cardiac toxicological functions, such as arrhythmia, hypertrophy, and failure (table S8).

Given increased expression of peptides with cytoskeletal ontologies, Ingenuity Pathway Analysis (IPA) was used to determine interaction networks. We observed age-associated up-regulation of vinculin as well as components within the vinculin interaction network in rhesus monkeys (Fig. 1C) and in rats (Fig. 2A). Figure 1D additionally depicts a vinculin-centric network of cardiac aging biomarkers whose deletion or mutation is also associated with cardiomyopathy in humans and thus may serve as therapeutic targets; to this end, table S9 annotates up-regulated cytoskeletal proteins in monkeys using comparative analysis with IPA and OMIM (Online Mendelian Inheritance in Man) (19), a human genetic phenotype database. Interventional or therapeutic regulators of all age–up-regulated proteins from Fig. 1B were identified by IPA and are presented in table S10; those that regulate vinculin, specifically, are in fig. S2.

Vinculin localization changes in aged rat ventricles

Relative to young (6 months) rats, aged (24 months) rats exhibited increased body weight, heart weight, and total cardiac output. However, heart weight and cardiac output normalized to body weight did not differ significantly (fig. S3), suggesting that they were undergoing physiological aging and nonpathological hypertrophy at this age. Echocardiograms revealed significant changes in diastolic and systolic LV internal dimension which resulted in a modest decrease in fractional shortening with advanced age (Fig. 2, B and C), as observed previously (20).

Age-related differences in vinculin localization were characterized by histology. Vinculin accumulated at IDs [connexin 43 $(Cnx43)^+$ pixels] and lateral borders ($Cnx43^-$ pixels) in aged rat myocardium, with an apparent preference at IDs (Fig. 2, D and E, and fig. S4, A to D), similar to observations in elderly human hearts (7). Vinculin binds to transmembrane proteins with its head domain and bundles or cross-links cortical F-actin with its tail domain, and is conserved across monkey, rat, and fly (fig. S5) (16, 21). Increased vinculin expression may reinforce the cortical actin superstructure, leading to measurable changes in cortical stiffness. Therefore, we performed atomic force microscopy (AFM)–based nanoindentation on isolated rat cardiomyocytes to probe cortical stiffness (fig. S6, A and B), which reflects cytoskeletal integrity or actin superstructure abundance and the degree of cross-linking by actin-binding proteins. There were no significant differences in stiffness between age groups (fig. S6C). However, isolated cells at these ages were poorly spread and minimally adherent, suggesting that isolation compromised cytoskeletal integrity.

Mechanical assessments reflecting in vivo physiology would benefit from use of an in situ model system that is characterized by preserved cytoskeletal structure and protein homology. It has been shown that the *D. melanogaster* heart meets these criteria (22–24). Thus, the rapidly aging fly allows for examination of cardiac remodeling over time without disruption of cytoskeletal integrity (Fig. 3).

Drosophila heart remodeling is genotype-dependent

The *Drosophila* heart consists of a bilateral row of cardiomyocytes that form a contractile tubular structure with a prominent anterior region called the conical chamber (Fig. 3A). To investigate age-associated cardiac remodeling, we first quantified changes in heart diameter in two common fly genotypes, yellow-white (*yw*) and white (w^{1118}) (Fig. 3B). Altered diameters are characteristic of cardiac remodeling. Diastolic diameter was significantly diminished at 5 weeks of age (aged) as compared to 1 week (adult) for both *yw* and w^{1118} (Fig. 3C), consistent with published results, which have suggested that diastolic restriction is a hallmark of cardiac aging in *Drosophila* (23, 24).

Intact *Drosophila* heart tubes can be prepared for AFM-based indentation to measure cortical stiffness without damaging tissue (fig. S7). A correlation between decreased diastolic diameters and increased cortical stiffness has been previously demonstrated in aging *Drosophila* and cardiomyopathy models (22, 24). Thus, we examined whether genotype-dependent changes in diastolic diameters with age correlated with stiffening. The conical chambers (Fig. 4A) of relaxed hearts were indented in situ at the ventral midline, proximal to IDs (Fig. 4B, 0 μm), and at distal positions, upon the costameres (Fig. 4B, 15 and 30 μm). Cardiomyocytes from 1-week flies had relatively homogeneous stiffness independent of genotype (Fig. 4C). However, *yw* exhibited cardiac stiffening, with preference to the ventral midline (Fig. 4C, green overlay), suggesting that excessive chamber remodeling correlates with increased cortical stiffness. This correlation between severe diastolic restriction and cortical stiffening was observed in a third *Drosophila* genotype, *white-Canton S* (*wCS*) (fig. S8), which demonstrated a cardiac aging phenotype similar to *yw*.

To examine the underlying contributors to cardiac stiffness in our system, *Drosophila* hearts were incubated in either blebbistatin, which inhibits actomyosin cross-bridge cycling, or cytochalasin D, which impairs cardiac contractility and depolymerizes cortical actin (25). Five-week *yw* exhibited a significant reduction in stiffness at the midline after blebbistatin treatment, but reduction was more pronounced in cytochalasin D–treated hearts (Fig. 4D and fig. S6D). These data suggest that increased resting tone in the relaxed heart does not exclusively account for the measured stiffness increase and that the state of the actin cytoskeleton may be a major component of age-related stiffening.

Expression differences in candidate actin-binding molecules were investigated from excised fly hearts using quantitative polymerase chain reaction (qPCR) to determine the molecular underpinnings of the age-associated changes. Most cytoskeletal gene transcripts were up-regulated with age in *yw*, including *Innexin-3* (152%), *Vinculin* (103%), α*Catenin-related* (99%), and α*Catenin* (58%). However, in w^{1118}, most of these gene transcripts did not change significantly (Fig. 4E and table S11). Furthermore, vinculin preference at the ID was

diminished in 5-week w^{1118} flies, which is in contrast to ID preference at all ages in *yw* flies and rats (Figs. 2E and 4F). These data, in conjunction with an observed lack of cortical stiffening, indicate that minimal cytoskeletal reinforcement occurs in w^{1118} with age as compared to *yw* or *wCS* (fig. S8).

Mechanical function is preserved in aging *Drosophila* hearts that undergo cytoskeletal remodeling

To determine whether increased passive stiffness is accompanied by altered active mechanics, we assessed the contractile dynamics of hearts beating against acute hemodynamic loads in situ. Precise measurements of shortening and lengthening intervals were made from high-speed videos (Fig. 5A), and the effect of load on heart wall velocities was assessed (Fig. 5B) (26). Shortening velocity is an index of relative force production. One-week w^{1118} flies had indistinguishable myocardial shortening velocities relative to age-matched *yw* flies ($P = 0.923$ for genotype, repeated-measures two-way ANOVA). However, w^{1118} velocities declined with age at all loads (Fig. 5C), whereas *yw* had preserved baseline shortening and lengthening velocities with age ($P = 0.96$, one-way ANOVA) (Fig. 5D). Relative cardiac power output during shortening, as calculated from Hill's equation (27) fit over the loads tested, was diminished to a greater degree with age in w^{1118} compared with *yw Drosophila* (fig. S9 and table S12).

These data indicate that mechanical performance is impaired in aged w^{1118} but is only evident under significant load for *yw*. Therefore, exaggerated diastolic restriction and cortical stiffening were not accompanied by contractile dysfunction; rather, restriction and stiffening correlated with preservation of baseline shortening and lengthening velocities. Correlation between vinculin expression and preserved contractility was also observed in *wCS* flies (fig. S8).

Vinculin overexpression recapitulates the age-related cortical stiffening phenotype

Our data suggest that cardiac vinculin overexpression is a conserved aging event, although its relationship to cardiac performance and organismal longevity remains unclear. Therefore, we first examined its functional consequences in *Drosophila*. Transgenes were strategically expressed in w^{1118} hearts, which did not stiffen with age, via the cardiac-specific tinHE-Gal4 driver (tinman heart enhancer) in conjunction with UAS-inducible *Vinculin* [vinculin heart-enhanced (*VincHE*)] or UAS–interfering RNA (RNAi) against *Vinculin* [vinculin knockdown (*VincKD*)] (Fig. 6A). Because decreased myosin and increased vinculin expression were both observed in our proteomic screen of rats and monkeys (Fig. 1C) and in HF patients (4), we also established a line in which hearts coexpress UAS-RNAi against *Myosin heavy chain* (*MhcKD*) and UAS-inducible *Vinculin*, dubbed *MhcKD + VincHE* (fig. S10), to determine whether vinculin overexpression could rescue dysfunction resulting from impaired myosin motor expression. *MhcKD + VincHE* flies were compared to both control and a line expressing only UAS-RNAi against *Myosin heavy chain* (*MhcKD*). Cardiac-specific qPCR verified knockdown and/or overexpression for each respective gene (fig. S11).

Structural and functional cardiac metrics were assessed in 1-week flies (Fig. 6A). Vinculin preferentially localized to IDs in all lines except *VincKD* (Fig. 6B). *VincHE* resulted in increased cardiac stiffness compared to controls, with preference at IDs, similar to 5-week *yw* (Fig. 6C). *MhcKD* exhibited reduced cardiac stiffness across the heart, consistent with results obtained using other transgene drivers (24). However, *MhcKD* + *VincHE* was indistinguishable from control, suggesting that vinculin overexpression could restore basal cardiac stiffness in hearts with myosin deficiency. Cytochalasin D treatment reversed the stiffening phenotype in *VincHE* (Fig. 6D) in a pattern matching 5-week *yw* (fig. S12), suggesting remodeling of the cardiac actin superstructure by increased vinculin. Increased vinculin expression, cortical stiffening, and similar response to drug treatments occurred in both w^{1118} hearts overexpressing vinculin (*VincHE*) and 5-week *yw*. These data indicate a causative role for vinculin in inducing age-related changes in *yw* hearts and correlate with age-associated cytoskeletal changes observed in rodents, monkeys, and humans.

Elevated vinculin expression improves heart function, myofilament organization, and life span

Heart dimensions and contractility were evaluated to examine the effects of vinculin overexpression on cell structure and function. *VincHE* had restricted cardiac diameters, although fractional shortening did not differ significantly from control (Fig. 6E). *MhcKD* hearts were significantly dilated and had impaired fractional shortening relative to control. Compensation for myosin knockdown with vinculin overexpression in *MhcKD* + *VincHE* flies partially restored heart dimensions and fractional shortening relative to control genotype's level. With regard to relative force production, *VincHE* myocardial shortening velocity was significantly higher at all loads and displayed a less severe load-dependent decline in fractional shortening versus all other genotypes (Fig. 6F). *MhcKD* heart wall velocities were diminished at all loads and resembled 5-week w^{1118} ($P = 0.19$, two-way ANOVA). However, *MhcKD* + *VincHE* hearts demonstrated substantially increased shortening velocity and increased relative cardiac power output compared to *MhcKD* and resembled controls (fig. S9 and table S12). Heart rate and period did not differ between *VincHE* and control and were depressed in *MhcKD*, but restored to control levels in *MhcKD* + *VincHE* (fig. S13). Moreover, cardiac-specific vinculin overexpression substantially prolonged median organismal life span by as much as 150% (Fig. 6G). These data suggest that *VincHE* hearts produce greater contractile forces, that vinculin overexpression can rescue diminished force production, and that cardiac-specific vinculin overexpression can increase longevity.

Computational studies have suggested a role for vinculin in regulating sarcomere lattice spacing and contractility (28). Therefore, electron micrographs of cross sections through *VincHE* and control cardiac myofibrils were examined to investigate alterations in ultrastructure (Fig. 7A and fig. S14). Thick-thick interfilament lattice spacing was similar in control and *VincHE* (average spacing of 45.74 and 45.79 nm, respectively) (Fig. 7B); however, a significant reduction in lattice spacing variance was observed for *VincHE* flies (3.11 nm for control versus 0.89 nm for *VincHE;* $P < 10^{-48}$, *F* test). A similar reduction in variance was observed for thick-to-thin interfilament spacing. These data suggest that

improved myofilament lattice order contributes to the enhanced cardiac contractility observed in *VincHE* flies.

DISCUSSION

Age-related HF results from chronic stressors that induce a heterogeneous array of physiological changes associated with overall negative outcome. However, individual events may be compensatory and required for maintaining function with age. Such events could be further promoted to treat failure or delay age-associated negative outcomes by therapeutic intervention in aging patients. An interrelationship between cytoskeletal composition and cell contractility has been presented recently (13), and postmortem analysis of age-associated HF corroborated altered expression of cytoskeletal proteins (7, 8). Although it is known that cytoskeletal molecules are crucial for cardiac function, a link between cytoskeletal remodeling and mechanical function has only been inferred (29) and not thoroughly vetted in aging cardiac systems. Our goal was to examine the contribution of cytoskeletal remodeling to function in aged organisms with varying myocardial complexity. Therefore, we integrated expansive proteomic analyses of mammals (rats and monkeys) with in-depth mechanistic analyses in a permissive invertebrate system (*Drosophila*). These data establish vinculin-mediated cytoskeletal remodeling as a regulator of myocardial structure and contractility during aging. Furthermore, therapeutic targets for age-related HF are proposed on the basis of their expression changes and known importance to cardiac function. In sum, these findings help clarify the role of the cortical cytoskeleton in cardiac aging and indicate vinculin and other mechanosensitive molecules as biomarkers of healthy or beneficial aging and as potential targets for therapeutic intervention in aging patients.

A primary aim was to assess conservation of age-related cytoskeletal remodeling and its impact on myocardial performance across species (simian, rat, and fly) during normal aging (as opposed to pathological conditions). The unique but complementary use of each chosen model allows for cooperative approaches to study aging networks or cellular functions of interest. Monkeys have a relatively long life span and cardiac physiology similar to humans, and rats are widely used as a human cardiac pathophysiology model. However, neither is optimally suited for mechanistic dissection of candidate proteins. In contrast, *D. melanogaster* is a rapidly aging organism, has extensive proteomic and cellular homology to murine models (30), and allows for tissue-specific genetic manipulation and experiments in which myocytes can be interrogated in situ with tools that directly visualize heart structure (24, 31, 32) or probe mechanics (22–24) without incurring damage to the heart (fig. S7). Cultured neonatal or stem cell–derived myocytes are often used to correlate mechanical and functional metrics (33, 34). However, such systems can lack adult morphology or mature cell junctions owing to remodeling of their intracellular structure (35) and altered contractility (36) in response to ex vivo extracellular cues, such as super-physiological substrate stiffness. Conversely, the *Drosophila* heart model allows us to examine the intersection of tensional and physiological homeostasis as a function of age and genetic manipulation with intact structures. Notably, genotype-dependent differences exist within *Drosophila*, similar to what has been observed between mouse strains (37), and thus, we selected two genotypes with diverse age-associated metrics (*yw* and w^{1118}) for comparison.

Conservation of vinculin-mediated cytoskeletal remodeling and its correlation with preserved mechanical function with age were also observed in *wCS*.

Vinculin was a promising candidate for investigation because it formed a central hub within the network of changes identified by proteomics as well as its known overexpression in aging human myocardium (6, 7). Additionally, vinculin has been implicated in integrin- (10) and cadherin-mediated (15) mechanotransduction and actin cytoskeletal interactions (21). Cardiac-specific vinculin deletion disrupts junctions and results in sudden death or cardiomyopathy in mice (38). Thus, vinculin is an appropriate first candidate to induce cytoskeletal remodeling, examine its effects on myocardial performance, and investigate a functional role in aging. Increased cardiac vinculin expression in flies correlated with greater localization at the cortical cytoskeleton, subsequent cytoskeletal reinforcement, and increased contractility. Partial rescue of impaired contractility and fractional shortening in *MhcKD* + *VincHE* also support a role for vinculin-mediated compensation for myo-filament dysfunction, as proposed previously (6). Although it has been suggested that cardiac cytoskeletal remodeling would result in stiffening and subsequent dysfunction (29), these data suggest that vinculin-mediated cytoskeletal reinforcement positively influences contractility and life span, as evidenced by elevated myocardial shortening velocities and the >150% increase in median life span in *VincHE* over control flies.

Vinculin overexpression may therefore be a conserved, beneficial hallmark of cardiac aging. Although the intrinsic molecular causes of vinculin overexpression in the aging heart remain unclear, upstream regulators and activating reagents have been identified that could be used for therapeutic vinculin overexpression. For example, growth differentiation factor 11 (GDF-11), a transforming growth factor–β family protein, positively regulates vinculin expression in the brain (39), and its overexpression can reverse pathophysiological hypertrophy in aged mice (3). However, GDF-11 declines with age in mice, and humans have lower concentrations of GDF-11 than mice at all ages (3), implying that reduced GDF-11 is not the underlying cause of vinculin overexpression in aging patients. Antagonism of miR-34, a negative transcriptional regulator of vinculin, led to improved outcome in mice experiencing pressure overload or myocardial infarction and correlated with vinculin overexpression (40), although vinculin was not specifically implicated as an active component of protection. Posttranslational modification of vinculin may also play a role in the aging process; vinculin localization is regulated by phosphorylation by the kinase *Abelson* (41), whose chronic inhibition by imatinib is associated with contractile dysfunction (42).

Vinculin is localized to costameres and IDs and plays separate but complementary roles for cell-matrix and cell-cell adhesion. Our data indicate that vinculin overexpression leads to cytoskeletal reinforcement, indicated by elevated cortical stiffness and increased myofilament lattice order (Fig. 7C). Because costameres directly couple Z discs to the membrane, increased vinculin could improve their integrity and ability to anchor myofilaments sufficiently and in correct orientation. These data are consistent with in vitro assessment of vinculin-null mouse myocytes, which had reduced cortical stiffness and increased interfilament spacing (28). Improved interfilament order may enhance the probability of actin-myosin cross-bridge formation, and thus the number of actively cycling

motors (43). Because the number of myosin heads engaged with thin filaments determines muscle performance (44), increased order predicts elevated probability of strongly bound myosin cross-bridges and resultant force production. Vinculin's role at cell-cell junctions, where it was preferentially localized in rats and flies, and where stiffness increased most significantly with age, is less clear. We hypothesize that ID-vinculin may help anchor myofibrils and facilitate longitudinal force transmission between myocytes, although additional studies are necessary to confirm this. Finally, crosstalk between the cortex and the Z disc, which is itself mechanosensitive (45), may also occur during remodeling and impact force production.

This study is limited to examination of vinculin-mediated cytoskeletal remodeling in *Drosophila* myocardium, where aging could be observed in a relatively short time. However, to more directly inform clinical outcomes, the contribution of vinculin overexpression to cardiac function should be further examined in larger mammalian models with physiology and life spans more similar to humans. In such models, a relationship between cardiac vinculin expression and clinically relevant functional metrics (pressure-volume relationship, ejection fraction, or electrocardiogram) and organismal life span may be demonstrated. Additionally, these studies can directly elucidate how vinculin affects diastolic and systolic performance in patient hearts. With regard to clinical application, our data suggest that vinculin overexpression alone may be sufficient to improve cardiac outcome during aging, indicating that intervention with vinculin mRNA may be a viable therapy. Application of vinculin-based gene therapies in preclinical models should be explored for their potential to prevent or delay age-related dysfunction. Future studies may also examine the efficacy of clinical treatment with previously identified vinculin regulators (enzymes, kinases, microRNAs, and small molecules) with emphasis on improving contractility while minimizing off-target effects to maximize cardiac protection. Such studies would set the stage for clinical trials. Currently, no trials exist to directly up-regulate vinculin in patient hearts. In studies concerning age-related HF without direct focus on vinculin, relative changes in its expression may serve as a biomarker or predictor of outcome. Finally, although vinculin was the primary focus of this study, our proteomic analysis reveals a wide array of biomarkers that warrant further investigation of their possible role in indicating outcome in HF patients or as therapeutic targets.

Here, we have outlined a cytoskeleton-based compensatory mechanism in the aging heart that is conserved across species. In presenting aging cardiac proteomes and providing a proof-of-concept study of vinculin in cardiac aging, we aimed to establish a resource that will facilitate a broader examination of cardiac aging so that additional therapeutic targets and regulators of aging heart function can be identified and validated. Our findings highlight the interplay of the molecular, cellular, and ultrastructural state of the cytoskeleton in maintenance of function in the aging heart and that studies of mechanotransduction can directly inform clinical outcomes. Furthermore, they can assist in developing integrated therapies to promote beneficial aging processes while preventing or suppressing maladaptive events to improve cardiac function in elderly patients.

MATERIALS AND METHODS

Study design

The aim of this study was to investigate the contribution of cytoskeletal remodeling to maintenance of function in aging myocardium and the broader hypothesis that aging is accompanied by conserved, compensatory events. Heart function is dependent on hierarchical organization of molecular and cellular components across multiple length scales. Therefore, we chose to perform an analysis that integrated complementary information across these scales. Recognizing a need for a comprehensive library of myocardial proteins with altered expression with age, we performed broad-spectrum proteomic analyses of the LV free wall in monkeys and in rats. Monkeys were chosen because of their physiological similarity to humans, and rats were selected because of their demonstrated use as a model of human cardiac aging. We used MS methods that enriched specifically for cellular/cytoskeletal constituents and not extracellular matrix components, given that age- (6, 7) and mutation-associated (17) cytoskeletal alterations have been associated with HF. Validation of MS data was performed in flies, a model organism that ages rapidly and in which genetic tools allow for examination of the contribution of specific network hits to cardiac function. Because this work used the fly heart as a model to study the mechanobiology of cardiac aging, we assessed the extent to which the model recapitulates mammalian cytoskeletal changes of interest by examining changes in cytoskeletal gene expression associated with age in humans. Subsequent data illustrate changes in form and function after vinculin-mediated cytoskeletal remodeling.

For all animals, ages were chosen on the basis of conventions for what constitutes post-development or adult and aged. One-week-old transgenic flies (Figs. 6 and 7) were examined to study the effects of cytoskeletal perturbations independent of aging. Flies of the appropriate age were selected randomly from larger populations for all experiments. Post hoc power analyses for the appropriate tests determined statistical power of at least 0.70 in mammals (Figs. 1 and 2) and at least 0.90 in flies (Figs. 3 to 7) given α of 0.05. Data were not blinded. No data were excluded from this study.

Vertebrate animals

Six adult (6 months) and six aged (24 months) female F344xBN F1 rats were obtained from the National Institute on Aging (NIA). Colony maintenance and experiments were performed in accordance with University of California, San Diego, Institutional Animal Care and Use Committee (IACUC) protocol S11032. Four adult (average, 11.63 years old; range, 8.75 to 14.12) and five aged (average, 22.4 years old; range, 18.81 to 25.48) male rhesus monkeys were maintained at the NIA in accordance with NIA IACUC protocol AG000238-07 (Effects of Aging on Experimental Atherosclerosis in Nonhuman Primates). Freshly isolated sections of LV rat myocardium were embedded in OCT and then flash-frozen in liquid nitrogen for subsequent histological analysis. Alternatively, rat and rhesus monkey samples where flash-frozen for subsequent proteomic analysis. Further details regarding echocardiography, cardiomyocyte isolation, and other mammalian experimental protocols are available in the Supplementary Materials.

Proteomic analysis of ventricular tissue

Heart tissues were prepared and analyzed by reversed-phase liquid chromatography tandem MS online with an Orbitrap Elite mass spectrometer (Thermo Scientific) coupled to an Easy-nLC 1000 system (Thermo Scientific), as described in Supplementary Materials and Methods. The analysis was operated in a data-dependent mode with full-scan MS spectra acquired at a resolution of 60,000 in the Orbitrap analyzer, followed by tandem mass spectra of the 20 most abundant peaks in the linear ion trap after peptide fragmentation by collision-induced dissociation. Database searching and processing are described in Supplementary Materials and Methods.

D. melanogaster lines, husbandry, and culture conditions

Fly lines were obtained from the Bloomington Drosophila Stock Center at Indiana University or the Vienna Drosophila RNAi Center. Flies were raised on standard agar-containing food at 25°C. Cardiac-specific perturbation of gene expression was achieved via the Gal4-UAS system as described previously (46). The UAS-Vinculin/UAS-MHC-RNAi line (*MhcKD* + *VincHE*) was generated through a series of crosses between the individual UAS lines and the balancer line *Cdc42/FM6;Sco/CyO* (fig. S10). Female progeny of tinHE-Gal4 and w^{1118} served as control. Proper transcription of both constructs was validated using heart-specific gene expression analysis (fig. S11 and table S11). Details regarding *Drosophila* stock information and cardiac analyses can be found in the Supplementary Materials. Fly microsurgery, as detailed in Supplementary Materials and Methods, did not influence passive or active measures of heart function (fig. S7).

Analysis of heart *D. melanogaster* parameters and performance under hemodynamic load

Ventrally exposed hearts were prepared as described in Supplementary Materials and Methods, arranged on a 35-mm petri dish, and imaged at 10× with a Hamamatsu electron multiplier charge-coupled device digital camera (100 to 150 fps) mounted on a Leica DM LFSA microscope. At least five contraction events were recorded per heart. Hearts were then submerged in 10% (w/v) Ficoll in oxygenated hemolymph, allowed to equilibrate for 1 min, and then imaged again. Hearts were then submerged in 20% (w/v) Ficoll in oxygenated hemolymph, equilibrated for 1 min, and then imaged once more. All hearts remained beating after completion of imaging. Generation of m-mode kymographs and subsequent calculation of systolic and diastolic lengths, fractional shortening, and shortening and lengthening velocities were performed with previously described software that has been modified to permit measurement of contraction and relaxation phases of individual systolic intervals (26). Shortening (contraction) and lengthening (relaxation) velocities were calculated by dividing the contraction distance by the contraction and relaxation intervals, that is, the time between the start of contraction and the start of isovolumic systole and the time between the end of isovolumic systole and the start of isovolumic diastole, respectively. A least squares fit was performed on the average shortening velocity for each genotype as a function of relative viscosity (MATLAB) based on Hill's equation (27). Fits are displayed over the viscosity ranges tested. Coefficients of the Hill equation are provided in table S12.

Statistical analyses

Data comparison was subjected to either a nonparametric Student's *t* test with unequal variance assumption, a Wilcoxon rank sum test, a repeated-measures one-way ANOVA, a one-way ANOVA with post hoc Tukey correction, or a two-way ANOVA with post hoc Tukey correction, as indicated in respective captions. Significance was assigned for $P < 0.05$. Scatter plots reflect the average measurement of individual animals with black bars indicating the mean. Pooled data are represented as means ± SEM unless otherwise indicated. All *Drosophila* experiments were performed with biological replicates of 15 to 38 flies unless otherwise indicated. All other experiments were performed with biological replicates of indicated sample size.

Supplementary Material

Refer to Web version on PubMed Central for supplementary material.

Acknowledgments

We thank G. Vogler, M. Nishimura, L. Cannon, J. Choi, and N. Alayari for technical assistance with *Drosophila* microsurgery and husbandry; D. Huang for assistance with echocardiography; D. B. Foster for discussions of MS; and R. Ross, J. Omens, and A. McCulloch for helpful insights regarding experimental protocols. Stocks obtained from the Bloomington Drosophila Stock Center (NIH P40OD018537) were used in this study.

Funding: This work was supported by grants from the NIH (HHSN268201000032C, P01HL077180, T32HL105373, R01AG045428, DP02OD006460, R01GM32443, R56HL124091, and R21HL106529), the American Heart Association (10SDG4180089 and 13PRE14410037), the American Federation for Aging Research, and intramural support from the NIA. A.S.T. is a fellow of the Rees-Stealy Research Foundation and the San Diego State University Heart Institute.

REFERENCES AND NOTES

1. Yancy CW, Jessup M, Bozkurt B, Butler J, Casey DE Jr, Drazner MH, Fonarow GC, Geraci SA, Horwich T, Januzzi JL, Johnson MR, Kasper EK, Levy WC, Masoudi FA, McBride PE, McMurray JJ, Mitchell JE, Peterson PN, Riegel B, Sam F, Stevenson LW, Tang WH, Tsai EJ, Wilkoff BL. American College of Cardiology Foundation; American Heart Association Task Force on Practice Guidelines. 2013 ACCF/AHA guideline for the management of heart failure: A report of the American College of Cardiology Foundation/American Heart Association Task Force on Practice Guidelines. J Am Coll Cardiol. 2013; 62:e147–e239. [PubMed: 23747642]
2. Sharma K, Kass DA. Heart failure with preserved ejection fraction: Mechanisms, clinical features, and therapies. Circ Res. 2014; 115:79–96. [PubMed: 24951759]
3. Loffredo FS, Steinhauser ML, Jay SM, Gannon J, Pancoast JR, Yalamanchi P, Sinha M, Dall'Osso C, Khong D, Shadrach JL, Miller CM, Singer BS, Stewart A, Psychogios N, Gerszten RE, Hartigan AJ, Kim MJ, Serwold T, Wagers AJ, Lee RT. Growth differentiation factor 11 is a circulating factor that reverses age-related cardiac hypertrophy. Cell. 2013; 153:828–839. [PubMed: 23663781]
4. Schaper J, Kostin S, Hein S, Elsässer A, Arnon E, Zimmermann R. Structural remodelling in heart failure. Exp Clin Cardiol. 2002; 7:64–68. [PubMed: 19649225]
5. van Berlo JH, Kanisicak O, Maillet M, Vagnozzi RJ, Karch J, Lin SC, Middleton RC, Marbán E, Molkentin JD. c-kit^{+} cells minimally contribute cardiomyocytes to the heart. Nature. 2014; 509:337–341. [PubMed: 24805242]
6. Hein S, Kostin S, Heling A, Maeno Y, Schaper J. The role of the cytoskeleton in heart failure. Cardiovasc Res. 2000; 45:273–278. [PubMed: 10728347]
7. Heling A, Zimmermann R, Kostin S, Maeno Y, Hein S, Devaux B, Bauer E, Klovekorn WP, Schlepper M, Schaper W, Schaper J. Increased expression of cytoskeletal, linkage, and extracellular proteins in failing human myocardium. Circ Res. 2000; 86:846–853. [PubMed: 10785506]

8. Birks EJ, Hall JL, Barton PJ, Grindle S, Latif N, Hardy JP, Rider JE, Banner NR, Khaghani A, Miller LW, Yacoub MH. Gene profiling changes in cytoskeletal proteins during clinical recovery after left ventricular-assist device support. Circulation. 2005; 112:I57–I64. [PubMed: 16159866]
9. Birks EJ. Molecular changes after left ventricular assist device support for heart failure. Circ Res. 2013; 113:777–791. [PubMed: 23989719]
10. Grashoff C, Hoffman BD, Brenner MD, Zhou R, Parsons M, Yang MT, McLean MA, Sligar SG, Chen CS, Ha T, Schwartz MA. Measuring mechanical tension across vinculin reveals regulation of focal adhesion dynamics. Nature. 2010; 466:263–266. [PubMed: 20613844]
11. Leerberg JM, Yap AS. Vinculin, cadherin mechanotransduction and homeostasis of cell–cell junctions. Protoplasma. 2013; 250:817–829. [PubMed: 23274283]
12. Holle AW, Tang X, Vijayraghavan D, Vincent LG, Fuhrmann A, Choi YS, del Álamo JC, Engler AJ. In situ mechanotransduction via vinculin regulates stem cell differentiation. Stem Cells. 2013; 31:2467–2477. [PubMed: 23897765]
13. Spanjaard E, de Rooij J. Mechanotransduction: Vinculin provides stability when tension rises. Curr Biol. 2013; 23:R159–R161. [PubMed: 23428328]
14. Danowski BA, Imanaka-Yoshida K, Sanger JM, Sanger JW. Costameres are sites of force transmission to the substratum in adult rat cardiomyocytes. J Cell Biol. 1992; 118:1411–1420. [PubMed: 1522115]
15. Huveneers S, de Rooij J. Mechanosensitive systems at the cadherin-F-actin interface. J Cell Sci. 2013; 126:403–413. [PubMed: 23524998]
16. Hirata H, Tatsumi H, Lim CT, Sokabe M. Force-dependent vinculin binding to talin in live cells: A crucial step in anchoring the actin cytoskeleton to focal adhesions. Am J Physiol Cell Physiol. 2014; 306:C607–C620. [PubMed: 24452377]
17. Vasile VC, Ommen SR, Edwards WD, Ackerman MJ. A missense mutation in a ubiquitously expressed protein, vinculin, confers susceptibility to hypertrophic cardiomyopathy. Biochem Biophys Res Commun. 2006; 345:998–1003. [PubMed: 16712796]
18. Spencer JL, Bhatia VN, Whelan SA, Costello CE, McComb ME. STRAP PTM: Software Tool for Rapid Annotation and Differential Comparison of Protein Post-Translational Modifications. Curr Protoc Bioinformatics. 2013; 13:13.22.1–13.22.36. [PubMed: 25422678]
19. Amberger JS, Bocchini CA, Schiettecatte F, Scott AF, Hamosh A. OMIM.org: Online Mendelian Inheritance in Man (OMIM), an online catalog of human genes and genetic disorders. Nucleic Acids Res. 2015; 43:D789–D798. [PubMed: 25428349]
20. Boluyt MO, Converso K, Hwang HS, Mikkor A, Russell MW. Echocardiographic assessment of age-associated changes in systolic and diastolic function of the female F344 rat heart. J Appl Physiol. 2004; 96:822–828. [PubMed: 14555689]
21. Tolbert CE, Burridge K, Campbell SL. Vinculin regulation of F-actin bundle formation: What does it mean for the cell? Cell Adh Migr. 2013; 7:219–225. [PubMed: 23307141]
22. Viswanathan MC, Kaushik G, Engler AJ, Lehman W, Cammarato A. A *Drosophila melanogaster* model of diastolic dysfunction and cardiomyopathy based on impaired troponin-T function. Circ Res. 2014; 114:e6–e17. [PubMed: 24221941]
23. Kaushik G, Zambon AC, Fuhrmann A, Bernstein SI, Bodmer R, Engler AJ, Cammarato A. Measuring passive myocardial stiffness in *Drosophila melanogaster* to investigate diastolic dysfunction. J Cell Mol Med. 2012; 16:1656–1662. [PubMed: 22225769]
24. Kaushik G, Fuhrmann A, Cammarato A, Engler AJ. In situ mechanical analysis of myofibrillar perturbation and aging on soft, bilayered *Drosophila* myocardium. Biophys J. 2011; 101:2629–2637. [PubMed: 22261050]
25. Rothen-Rutishauser BM, Ehler E, Perriard E, Messerli JM, Perriard JC. Different behaviour of the non-sarcomeric cytoskeleton in neonatal and adult rat cardiomyocytes. J Mol Cell Cardiol. 1998; 30:19–31. [PubMed: 9500878]
26. Cammarato A, Ocorr S, Ocorr K. Enhanced assessment of contractile dynamics in *Drosophila* hearts. Biotechniques. 2015; 58:77–80. [PubMed: 25652030]
27. Hill AV. The heat of shortening and the dynamic constants of muscle. Proc R Soc Lond B Biol Sci. 1938; 126:136–195.

28. Tangney JR, Chuang JS, Janssen MS, Krishnamurthy A, Liao P, Hoshijima M, Wu X, Meininger GA, Muthuchamy M, Zemljic-Harpf A, Ross RS, Frank LR, McCulloch AD, Omens JH. Novel role for vinculin in ventricular myocyte mechanics and dysfunction. Biophys J. 2013; 104:1623–1633. [PubMed: 23561539]
29. Perriard JC, Hirschy A, Ehler E. Dilated cardiomyopathy: A disease of the intercalated disc? Trends Cardiovasc Med. 2003; 13:30–38. [PubMed: 12554098]
30. Cammarato A, Ahrens CH, Alayari NN, Qeli E, Rucker J, Reedy MC, Zmasek CM, Gucek M, Cole RN, Van Eyk JE, Bodmer R, O'Rourke B, Bernstein SI, Foster DB. A mighty small heart: The cardiac proteome of adult Drosophila melanogaster. PLOS One. 2011; 6:e18497. [PubMed: 21541028]
31. Ocorr K, Reeves NL, Wessells RJ, Fink M, Chen HS, Akasaka T, Yasuda S, Metzger JM, Giles W, Posakony JW, Bodmer R. KCNQ potassium channel mutations cause cardiac arrhythmias in *Drosophila* that mimic the effects of aging. Proc Natl Acad Sci USA. 2007; 104:3943–3948. [PubMed: 17360457]
32. Wolf MJ, Amrein H, Izatt JA, Choma MA, Reedy MC, Rockman HA. *Drosophila* as a model for the identification of genes causing adult human heart disease. Proc Natl Acad Sci USA. 2006; 103:1394–1399. [PubMed: 16432241]
33. Zhang J, Klos M, Wilson GF, Herman AM, Lian X, Raval KK, Barron MR, Hou L, Soerens AG, Yu J, Palecek SP, Lyons GE, Thomson JA, Herron TJ, Jalife J, Kamp TJ. Extracellular matrix promotes highly efficient cardiac differentiation of human pluripotent stem cells: The matrix sandwich method. Circ Res. 2012; 111:1125–1136. [PubMed: 22912385]
34. Sheehy SP, Grosberg A, Parker KK. The contribution of cellular mechanotransduction to cardiomyocyte form and function. Biomech Model Mechanobiol. 2012; 11:1227–1239. [PubMed: 22772714]
35. Jacot JG, McCulloch AD, Omens JH. Substrate stiffness affects the functional maturation of neonatal rat ventricular myocytes. Biophys J. 2008; 95:3479–3487. [PubMed: 18586852]
36. Hazeltine LB, Simmons CS, Salick MR, Lian X, Badur MG, Han W, Delgado SM, Wakatsuki T, Crone WC, Pruitt BL, Palecek SP. Effects of substrate mechanics on contractility of cardiomyocytes generated from human pluripotent stem cells. Int J Cell Biol. 2012; 2012:508294. [PubMed: 22649451]
37. Barrick CJ, Rojas M, Schoonhoven R, Smyth SS, Threadgill DW. Cardiac response to pressure overload in 129S1/SvImJ and C57BL/6J mice: Temporal- and background-dependent development of concentric left ventricular hypertrophy. Am J Physiol Heart Circ Physiol. 2007; 292:H2119–H2130. [PubMed: 17172276]
38. Zemljic-Harpf AE, Miller JC, Henderson SA, Wright AT, Manso AM, Elsherif L, Dalton ND, Thor AK, Perkins GA, McCulloch AD, Ross RS. Cardiac-myocyte-specific excision of the vinculin gene disrupts cellular junctions, causing sudden death or dilated cardiomyopathy. Mol Cell Biol. 2007; 27:7522–7537. [PubMed: 17785437]
39. Williams G, Zentar MP, Gajendra S, Sonego M, Doherty P, Lalli G. Transcriptional basis for the inhibition of neural stem cell proliferation and migration by the TGFβ-family member GDF11. PLOS One. 2013; 8:e78478. [PubMed: 24244313]
40. Bernardo BC, Gao XM, Winbanks CE, Boey EJ, Tham YK, Kiriazis H, Gregorevic P, Obad S, Kauppinen S, Du XJ, Lin RC, McMullen JR. Therapeutic inhibition of the miR-34 family attenuates pathological cardiac remodeling and improves heart function. Proc Natl Acad Sci USA. 2012; 109:17615–17620. [PubMed: 23047694]
41. Bays JL, Peng X, Tolbert CE, Guilluy C, Angell AE, Pan Y, Superfine R, Burridge K, Demali KA. Vinculin phosphorylation differentially regulates mechanotransduction at cell–cell and cell–matrix adhesions. J Cell Biol. 2014; 205:251–263. [PubMed: 24751539]
42. Hu W, Lu S, McAlpine I, Jamieson JD, Lee DU, Marroquin LD, Heyen JR, Jessen BA. Mechanistic investigation of imatinib-induced cardiac toxicity and the involvement of c-Abl kinase. Toxicol Sci. 2012; 129:188–199. [PubMed: 22641616]
43. Farman GP, Walker JS, de Tombe PP, Irving TC. Impact of osmotic compression on sarcomere structure and myofilament calcium sensitivity of isolated rat myocardium. Am J Physiol Heart Circ Physiol. 2006; 291:H1847–H1855. [PubMed: 16751283]

44. Piazzesi G, Reconditi M, Linari M, Lucii L, Bianco P, Brunello E, Decostre V, Stewart A, Gore DB, Irving TC, Irving M, Lombardi V. Skeletal muscle performance determined by modulation of number of myosin motors rather than motor force or stroke size. Cell. 2007; 131:784–795. [PubMed: 18022371]

45. Hoshijima M. Mechanical stress–strain sensors embedded in cardiac cytoskeleton: Z disk, titin, and associated structures. Am J Physiol Heart Circ Physiol. 2006; 290:H1313–H1325. [PubMed: 16537787]

46. Brand AH, Perrimon N. Targeted gene expression as a means of altering cell fates and generating dominant phenotypes. Development. 1993; 118:401–415. [PubMed: 8223268]

47. Deutsch EW, Mendoza L, Shteynberg D, Farrah T, Lam H, Tasman N, Sun Z, Nilsson E, Pratt B, Prazen B, Eng JK, Martin DB, Nesvizhskii AI, Aebersold R. A guided tour of the Trans-Proteomic Pipeline. Proteomics. 2010; 10:1150–1159. [PubMed: 20101611]

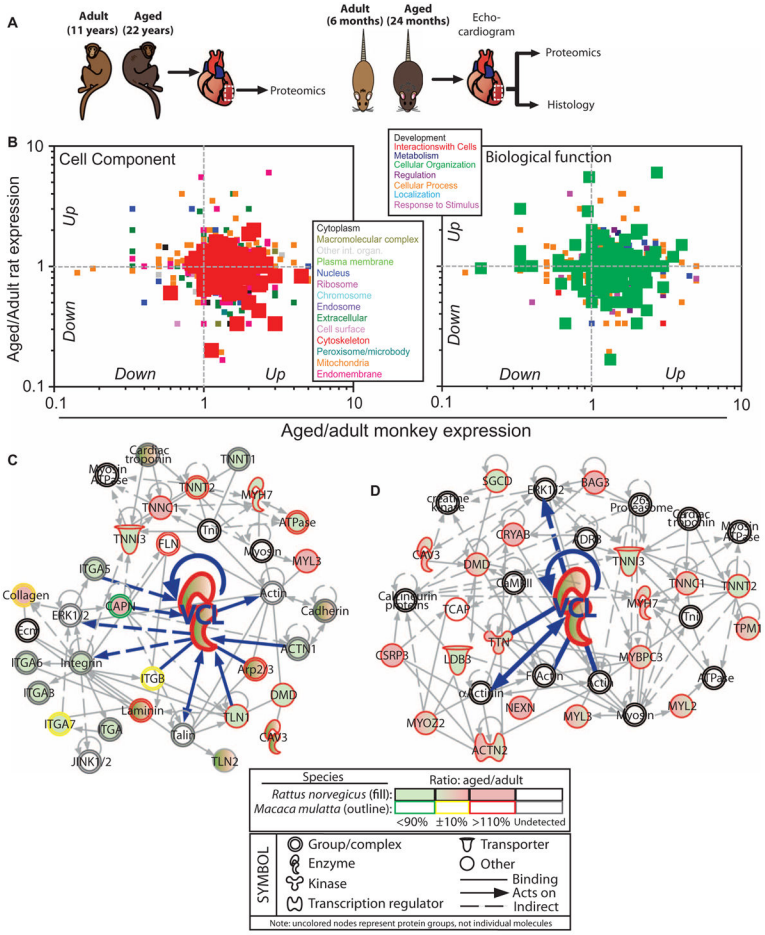

Fig. 1. Comparison of cardiac proteomes of ventricles from adult and aged simians and rats to identify cardiac aging biomarkers

(**A**) Experimental design to analyze LV free wall (dashed white box) from intact hearts from aged and adult simians and rats. (**B**) Scatter plot of the ratio of aged to adult spectral counts. Each point represents the ratio for a single protein, and colors indicate cell component category (left) or biological function (right) into which each protein falls, as determined by STRAP analysis. (**C**) IPA for sarcomeric and cytoskeletal proteins yielded network interactions. Protein expression determined by spectral counting for rats is denoted by filled symbols, while simian protein expression is an outlined symbol. Color coding of expression is shown below with a legend for shapes and interactions. Vinculin (VCL) and vinculin-specific interactions are highlighted by bold, blue lines within the network. (**D**) Network of cardiomyopathy-associated proteins that are up-regulated with age in monkeys. Annotations obtained using IPA and OMIM are available in table S9. Note that uncolored nodes represent protein groups or complexes, not individual or redundant molecules.

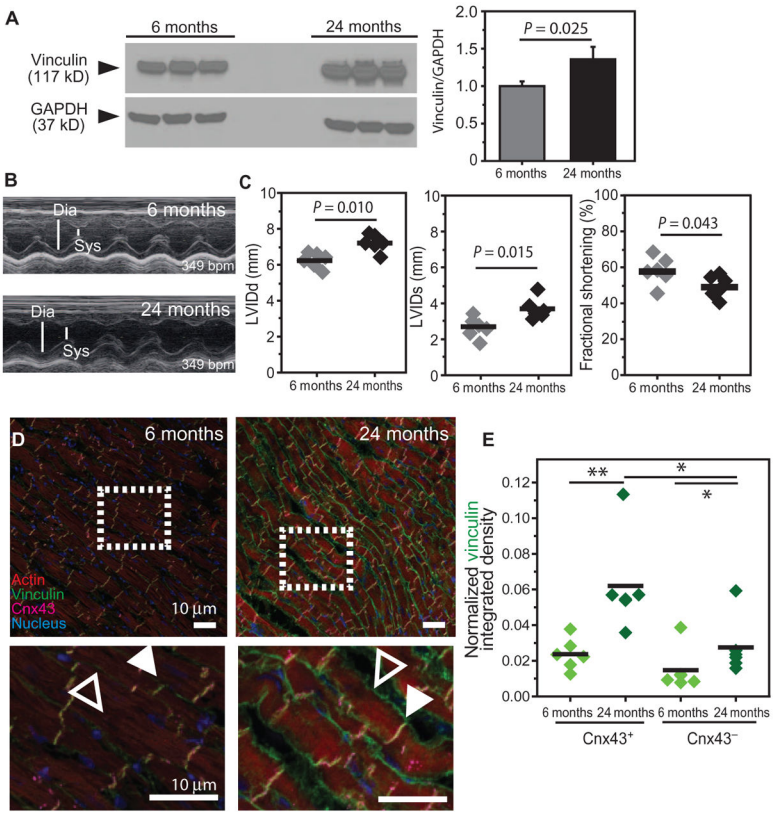

Fig. 2. Cytoskeletal remodeling in adult and aged rats with ventricular hypertrophy but preserved fractional shortening

(**A**) Western blot for vinculin from LV free wall and quantification of normalized blot intensity [vinculin/GAPDH (glyceraldehyde-3-phosphate dehydrogenase)] for each age cohort. Shown are three technical replicates of six pooled samples at the indicated ages. *P* value determined by unpaired, nonparametric *t* test. (**B**) LV echocardiograms displaying diastolic (Dia) and systolic (Sys) chamber widths for the indicated ages. (**C**) LV end diastolic and systolic diameters (LVIDd and LVIDs, respectively) and fractional shortening were measured from kymographs in (B) for the indicated ages. (**D**) Staining for vinculin, Cnx43, actin, and nuclei [DAPI (4′,6-diamidino-2-phenylindole)] in the rat ventricular myocardium. Dashed boxes indicate the magnified areas below. Filled arrowheads indicate IDs; open arrowheads indicate transverse junctions. Scale bars, 10 µm. (**E**) Vinculin expression with age at both IDs ($Cnx43^+$ pixels) and lateral junctions ($Cnx43^-$ pixels) as quantified using a method outlined in fig. S4. In (C) and (E), $*P < 0.05$, $**P < 0.01$, or otherwise indicated, by Wilcoxon rank sum test.

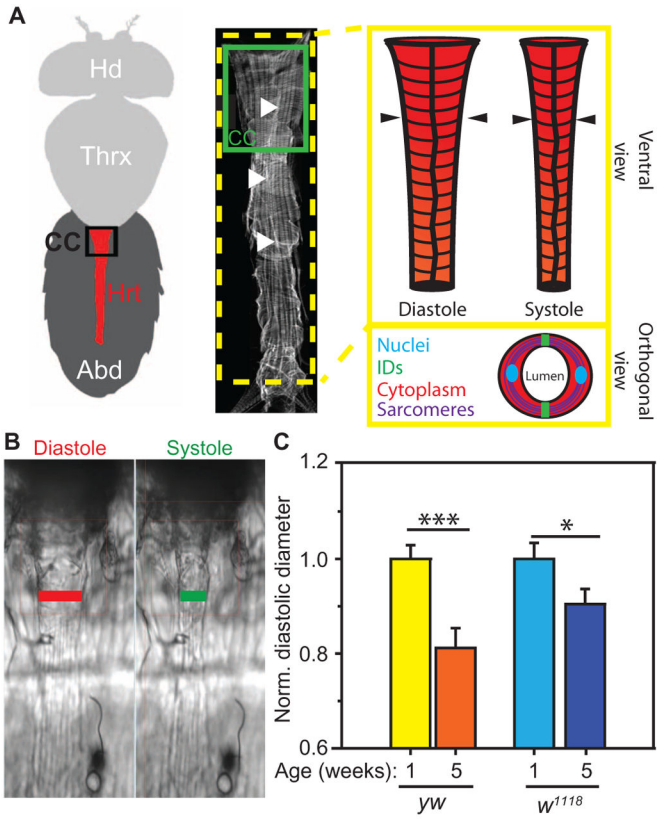

Fig. 3. Age- and genotype-associated structural remodeling in the *Drosophila* heart

(**A**) Ventral cartoon and confocal microscopy view of the *Drosophila* head (Hd), thorax (Thrx), and abdomen (Abd). Abdomen contains the heart (Hrt; red), whose major contractile compartment is the conical chamber (CC). Image modified from (30). Filled arrowheads indicate the cell-cell junctions or IDs along the middle axis of the heart. Illustration of heart during diastole versus systole. Arrowheads indicate the region of the heart measured in (B). Inset illustration shows an orthogonal view through the heart indicating the bilateral myocytes with components of interest highlighted. (**B**) Images of hearts captured from a 120-fps movie used for physiological assessments. Lines indicate where diastolic and systolic dimensions and phases were measured unless otherwise noted. (**C**) Heart diameters for the indicated *Drosophila* genotypes and ages (*yw*, yellow-white; w^{1118}, white) normalized to the genotype-specific 1-week diameter. Data are normalized averages ± SEM ($n > 20$). *$P < 0.05$, ***$P < 0.001$, unpaired, nonparametric *t* tests.

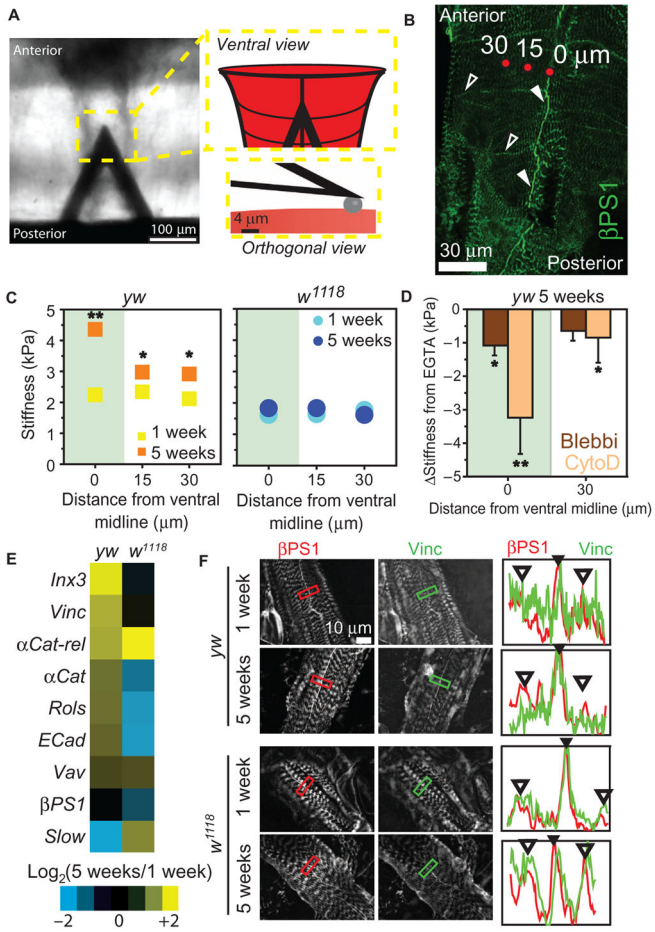

Fig. 4. Age-associated heart stiffening correlates with cortical actin cytoskeletal remodeling in flies

(**A**) AFM cantilever positioned above the *Drosophila* heart. Insets are illustrations of a cantilever over the heart (top) and spherical indenter (bottom). (**B**) βPS1 localizes within hearts at IDs (filled arrowheads) and lateral junctions (open arrowheads) along the length of the fly heart. AFM indentation locations are indicated by red dots and their distance from ventral midline (0, 15, or 30 μm). (**C**) Cardiac stiffness as a function of distance from ventral mid-line in *yw* and w^{1118} flies (average ± SEM, $n > 20$). *$P < 0.05$, **$P < 0.01$ for 5-week versus 1-week at respective distance, using non-parametric *t* tests. Green overlay indicates ventral midline data. (**D**) Change in cardiac stiffness for 5-week *yw* after indicated pharmacological treatment. Data are individual flies with mean change in stiffness from EGTA ± SD ($n = 10$ per treatment). *$P < 0.05$, **$P < 0.01$, versus mean stiffness in EGTA using a repeated-measures one-way analysis of variance (ANOVA). (**E**) Ratio of aged (5-week) to adult (1-week) gene expression in the heart ($n = 3$ biological replicates of 10 pooled hearts per age and genotype). (**F**) Immunohistochemistry of hearts from 1- and 5-week flies showing vinculin or β_1 integrin expression. Plots indicate fluorescence intensity from a line drawn within the box in each image for vinculin (green) or β_1 integrin (red). Filled arrowheads indicate ID; open arrowheads, costameres.

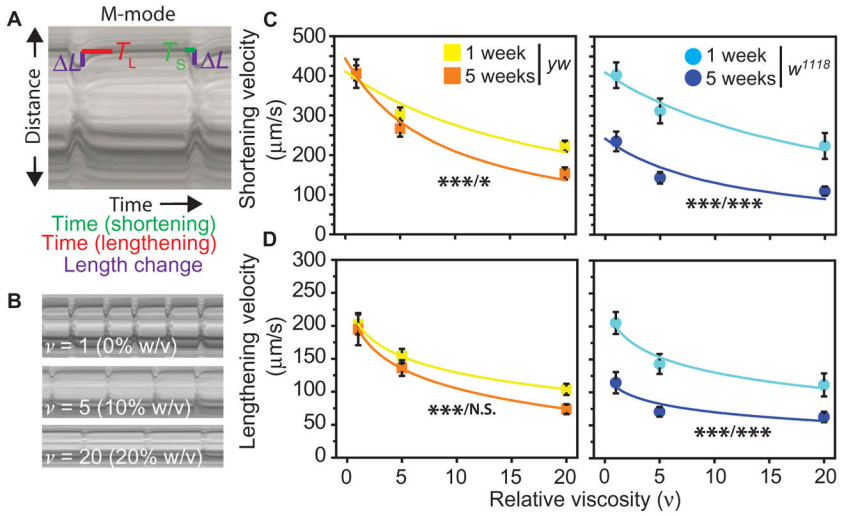

Fig. 5. Cytoskeletal remodeling correlates with the preservation of genotype-specific basal cardiomyocyte shortening during aging

(**A**) Motion-mode (M-mode) kymographs of fly hearts indicating where time of shortening phase (T_S, green), lengthening phase (T_L, red), and heart width change (ΔL) are measured. Purple lines indicate the half ΔL or movement of one side of the heart wall. (**B**) M-mode images of a heart sequentially placed under hemodynamic or viscous loading with relative viscosities (ν) indicated. (**C** and **D**) Shortening (C) and lengthening (D) velocities were calculated from the difference in heart width between systole and diastole and time interval (shortening = $2\Delta L/T_S$; lengthening = $2\Delta L/T_L$). Data are average velocities ± SEM for the indicated genotypes and ages as a function of hemolymph viscosity ($n > 29$ for each age, genotype, and load). Shortening velocity is fit with Hill's equation for muscle, whereas lengthening velocity is fit with a general log function for illustrative purposes. *$P < 0.05$ and ***$P < 0.001$ using two-way ANOVA, where asterisks indicate P values for difference in velocity as a function of viscosity and age, respectively (that is, viscosity/age). N.S., not significant.

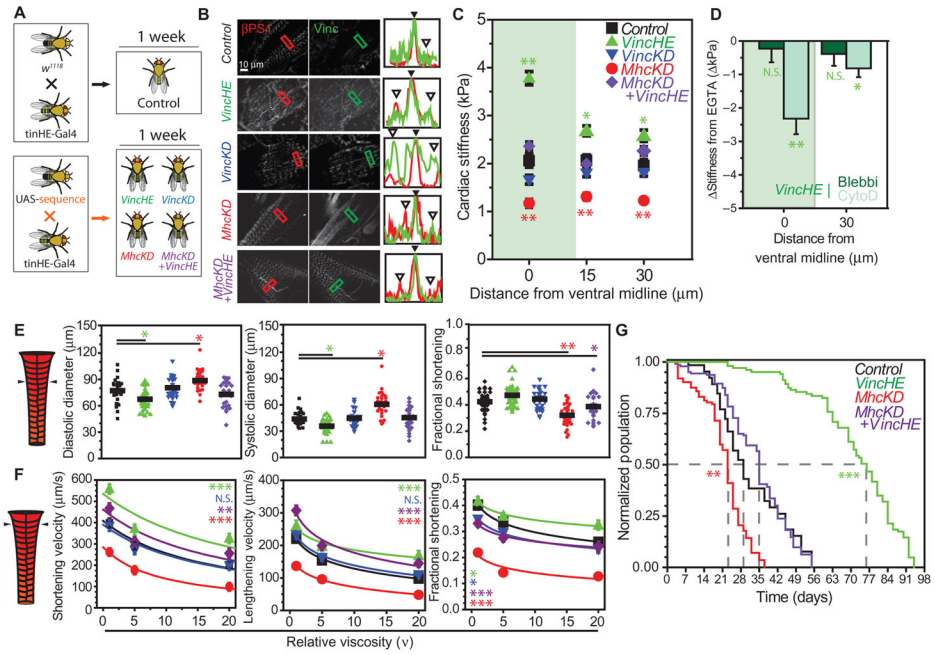

Fig. 6. Cardiac-specific cytoskeletal reinforcement results in increased cardiac contractile function and extends *Drosophila* life span

(**A**) Illustration of crosses used to generate control and transgenic lines. (**B**) Immunohistochemistry of βPS1 and vinculin in 1-week-old genotypes. Plots indicate fluorescence intensity from line drawn within box in each image for vinculin (green) or βPS1 (red). Filled arrowheads indicate ID; open arrowheads, costameres. (**C**) Cardiac stiffness as a function of distance from the ventral midline. Data are averages ± SEM (n > 20). (**D**) Change in cardiac stiffness from EGTA after indicated pharmacologic treatment. Data are means ± SD (n = 10). Ventral midline indicated by green overlay. (**E**) At the indicated position, genotypes in (A) were assessed for heart diameters and fractional shortening. Data are individual flies with mean indicated. In (C) to (E), *P < 0.05, **P < 0.01, compared to control by one-way ANOVA. (**F**) Heart wall velocities and fractional shortening assessed under viscous load and fit by Hill's model (shortening velocity) or a general log fit (lengthening velocity, fractional shortening, for illustration purposes). Data are means ± SEM (n > 29). *P < 0.05, **P < 0.01, ***P < 0.001, N.S. (not significant) comparing indicated genotype and control (black), two-way ANOVA. (**G**) Survival curves for indicated genotypes (n > 100). Gray lines indicate time in days to which 50% of starting population survived. **P < 0.01, ***P < 10^{-6} for population over time versus control, two-way ANOVA. P = 0.025 for *MhcKD* + *VincHE* versus *MhcKD* (two-way ANOVA).

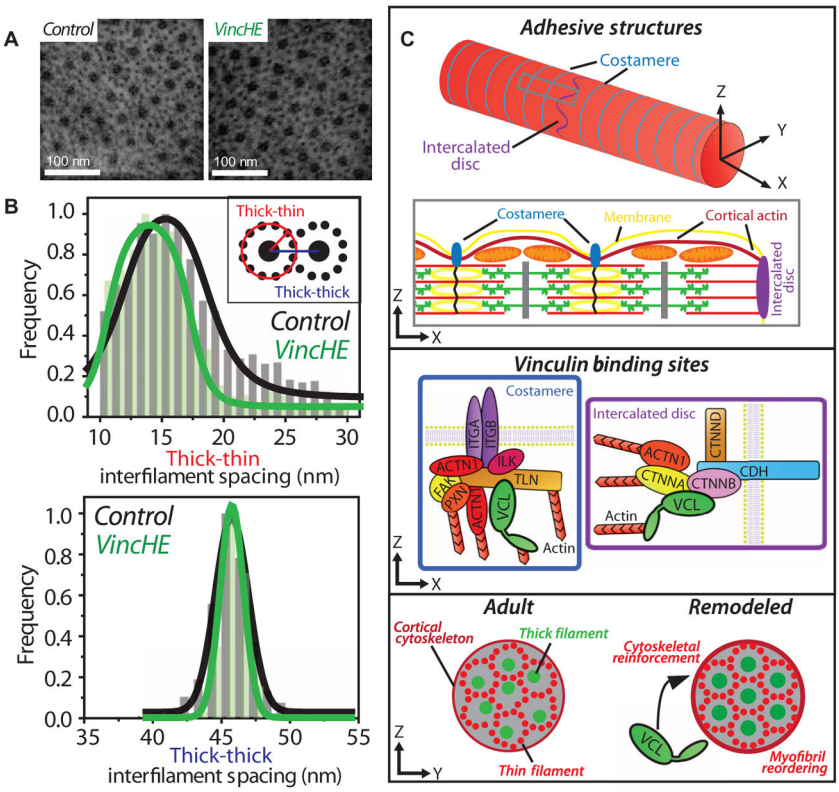

Fig. 7. A proposed role for cytoskeletal regulation of myofilament order and contracility in the aging myocyte

(**A**) Representative transmission electron microscopy (TEM) micrographs of myofibril cross sections of 1-week control (black) and *VincHE* (green) flies. (**B**) Interfilament spacing analysis as outlined in fig. S14. Inset image illustrates how distances were measured. Data are histograms indicating distribution of interfilament spacing with Gaussian fits, $n = 480$ (control) and $n = 670$ (*VincHE*) thick filaments. (**C**) Top: Adult cardiac myocytes (fly, rodent, monkey, and human) have defined cell-cell and cell-matrix junctions, referred to as IDs and costameres, respectively. Costameres couple Z discs to the membrane and cross-link the cortical actin cytoskeleton. The terminal sarcomere ends at the ID, rather than a Z disc, which is populated by actin-based adherens junctions as well as desmosomal and gap junctions. Middle: Vinculin binds to integrin and cadherin complexes and can facilitate remodeling of the actin superstructure by nucleating and bundling F-actin via its tail domain. Bottom: Vinculin is overexpressed with age. We propose that this results in reinforcement of the cortical cytoskeleton via cell junctions, which in turn may have propagating mechanical effects through the myofilament lattice that supports or enhances its crystalline order. Thus, the cortical cytoskeleton can act as an extrasarcomeric regulator of myocyte structure and contractile function. Simplified schematic shown. Proteins indicated by gene name.